ISSN 1330-3651 (Print), ISSN 1848-6339 (Online) https://doi.org/10.17559/TV-20230720000818
Original scientific paper

Implementation of Wiener Algorithm for Spectral Reflectance Reconstruction of 3 and 6 Channel Images

Andrej UČAKAR*, Primož WEINGERL, Andrej KOŠIR, Aleš HLADNIK

Abstract: Wiener estimation is a widely used technique for the spectral reflectance reconstruction of colored objects. In our study the reflectance estimation of 3-channel images acquired using traditional RGB camera was compared with that of 6-channel images captured by a modified 6-channel camera. 240 patches of ColorChecker DC Chart were used for training and testing of the models.Their performance was assessed via quality metrics *PSNR*, *RMSE* and CIE *DE*2000 based on the reconstructed and spectrophotometrically measured reflectance values. Compared to the 3-channel models, 6-channel models in general provided better results. Lowest color difference CIE *DE*2000 was obtained when using 10 calculation terms in the 3-channel algorithm and 13 terms in the 6-channel. Best reconstruction models, i.e. lowest CIE *DE*2000 and *RMSE* and highest *PSNR* values, were found for the skin and neutral tones while the performance was the poorest with the saturated color patches. The obtained results can be of use in various practical applications, such as in a printing workflow with high precision color rendering or for accurate digitization of paintings and other works of art.

Keywords: color accuracy; machine learning; spectral reflectance reconstruction; Wiener estimation

1 INTRODUCTION

Devices used in a digital graphic workflow such as conventional three-channel digital cameras have been engineered to emulate the spectral integration found within the human visual system [1]. Such devices generally work successfully in a number of practical applications, but problems arise when the reproductions are printed and viewed under different light sources or shown on computer displays under varying light conditions. In colorimetry, metamerism is a perceived matching of colors with different (nonmatching) spectral power distributions. Colors that match this way are called metamers. Metamerism can also occur due to the change of the observer, as people generally differ from each other in terms of the sensitivity of the cones to the light of individual wavelengths.

One solution to the problems associated with a metameric reproduction workflow or mismatch in the perception of colors between the original and the reproduction is provided by the systems for spectral imaging. These systems make it possible that the color of the observed object is expressed by its physical properties, such as a reflection spectrum which is independent of the light source for object illumination, as well as of the observer or capturing device.

Spectral imaging is defined as acquisition, processing, displaying and interpreting image data with a larger number of spectral channels, so a spectral image is an image which has tens of components, whereas a conventional RGB image has three. The visible light (380 - 780 nm) spectrum is sampled with a suitable (e.g., 5 nm) wavelength interval. This leads to a more accurate reproduction of colors in digital form [2-4].

A high quality estimation of the spectral reflectance is required in digital archives, network museums, e-commerce and telemedicine, for restoration and conservation in the field of cultural heritage [5-9], remote sensing [10, 11], forestry and geology, biomedical research, quality control in industry, medicine in determining the presence of melanin and haemoglobin [12], astronomy [13], in a printing workflow with high precision color rendering [14]. The field of fine art paintings has recently been intensively studied because systems for very precise digitization bring many advantages (accurate digital archiving).

Numerous recent studies demonstrate that conventional digital still RGB cameras can be successfully used to provide high-quality color information about the imaged object or scene [14]. This can typically be accomplished by performing the colorimetric camera characterisation, a procedure that maps the device-dependent (= camera RGB values) into a device-independent (CIEXYZ or CIELab) color space [16].

Two approaches are applicable: the model-based one focuses on a mathematical description of the physical process by which the device captures or renders colors [17]. This method requires the camera sensor sensitivities to be known in advance. Alternatively, in a target-based (= empirical) approach the camera itself is considered a black box and the information on a number of colored patches is obtained by both the camera and the color measuring device, usually a spectrophotometer. Mapping of the RGB into CIEXYZ (or CIELab) values is accomplished via the creation of a suitable colorimetric characterization model). Finally, the computed colorimetric values are compared to those obtained by the spectrophotometer and the performance of the model, i.e., the reconstruction accuracy, is assessed by means of various performance metrics, such as *RMSE*, *PSNR* or a color difference formula.

One of the problems associated with the above described three-to-three color space transformation that converts an RGB camera into a spatial colorimeter is that the computed CIEXYZ values are still illuminant-dependent [20]. On the other hand, in a multi-channel imaging system that is based on the responses of several (three or more) color channels, one attempts to recover spectral information about the imaged samples. When such a strategy is successful, the multi-channel camera can be seen as a spectrophotometer that is able to capture device as well as illuminant-independent images. The spectral camera

characterization is therefore based on the estimation (or reconstruction) of reflectance spectra, i.e., on the mapping of a low-dimensional into a higher-dimensional space consisting typically of 72 (wavelengths between 380 and 730 nm in 5 nm steps) discrete reflectance values. Such an approach that utilizes relatively few color channels is possible [18, 19], due to the fact that the spectral properties of most surfaces are relatively smooth functions of wavelength [22, 23].

Since the number of image sensor responses is typically much smaller compared to the number of spectral bands to be reconstructed, spectral reconstruction is, in principle, an ill-posed problem. Several state of the art approaches for the spectral reconstruction are described in the literature: Pseudoinverse [24], Imai-Berns [25], POCS [26], Kernel [27] and Wiener [28] method. Wiener estimation is one of the simpler transformation methods that has been reported to provide accurate reconstructions [28].

In our study we, while adopting traditional predictive machine learning concepts, chose the combination of model- and target-based approach. We captured colors with known reflectance to construct a response-to-reflectance transformation using Wiener filter for the estimation of patches' reflectance. For the reconstruction quality assessment, we calculated *PSNR*, *RMSE* and *DE*2000 from the measured and reconstructed reflectance values. The goal of this paper was to assess the algorithm performance based on 3 and 6 channel input images when applied to saturated, neutral and skin tones. In additon, the impact of the number of terms used in the Wiener estimation was also studied.

2 MATERIALS AND METHODS

2.1 3 and 6 Channel Cameras

The three-channel digital camera used in the study was Sinarback 54 (Fig. 1) which features a Kodak sensor KAF-22000CE CCD with a resolution of 5440 × 4880 pixels. This is a full-frame color image sensor consisting of 9 µm × 9 µm pixels. Each pixel is covered by one of the red, green, or blue filters. The red, green, and blue pixels are arranged based on a Bayer pattern, so the number of green pixels is twice the number of red or blue ones. The Sinar CaptureShop 6.0.2 software was used to drive the camera in single-shot mode. This software has its own internal interpolation algorithm for deriving RGB values at each pixel. Such post processing can affect the results of gain calculations and other characteristic factors of the camera. To avoid confounding the experimental results, only raw output files were analyzed.

Figure 1 Sinar Back 54FO camera

Sinar CaptureShop was not utilized for interpolation or other image processing routines. The Sinarback 54 camera has a 14-bit ADC circuit, so output digital counts are in the range of 0 to 16383 ($2^{14} - 1$).

For capturing 6-channel images we applied a modified conventional Sinarback 54H digital camera (Technische Universität Darmstadt, Institute of Printing Science and Technology) [29]. Camera's built-in IR cut-off filter was removed and replaced with a clear BK7 glass. Unaxis visible-spectrum bandpass filter was used in front of the camera lens [30]. This increased the range of wavelength sensitivity compared with the Sinar's IR filter. With our modified camera we intended to simulate the original Sinarback filter by imaging through a Schott BG39 glass filter with a thickness of 3 mm.

The scheme of the modified Sinarback 54 camera and associated optics is shown in Fig. 2. The Unaxis filter was placed at the end of the lens shade. The shade was tilted to prevent inter-reflections between the filter and lens. The filter holder was fabricated using black foamcore.

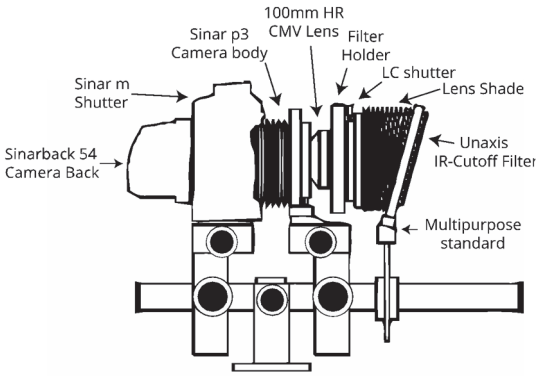

Figure 2 Scheme of the modified Sinar Back 54FO camera

2.2 Color Chart

There are several common targets available for the colorimetric camera characterisation; we utilized the Xrite ColorChecker DC which contains 240 color patches (Fig. 3).

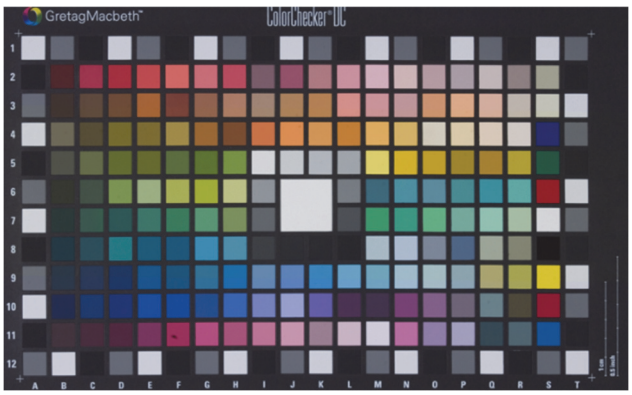

Figure 3 Color Checker DC color chart

2.3 Obtaining 6 Channel Images

Capturing a 6-channel image is, unlike that of a 3-channel one, not a trivial process since a modified camera is used. The scene was illuminated using Broncolor Xenon Strobe lamp as evenly as possible, camera settings were set to manual (ISO, aperture, sharpness, ...). The

image processing procedure consists of two main steps (Fig. 4).

2.3.1 Camera-Based Image Processing

The camera back has micro-positioning capabilities, so the sensor is moved four times to position each color of the Bayer patterned color filter array over each pixel's spatial location. This is known as the "four shot" or "four pop" mode and results in full color images without spatial interpolation but can only be used for static scenes. The four shots were repeated with each filter in front of the lens, resulting in an "eight shot" or "eight pop" mode. Capture was controlled by a modified version of Sinar's CaptureShop software. For each exposure time, the software captured an image with the shutter closed and subtracted this "dark image" from subsequent exposures. The software also applied a multiplicative spatial correction called the sensor shading reference that compensated for pixel-wise differences in the camera's gain. The resulting eight-plane image was stored in Sinar's, TIFF based, STI file format.

2.3.2 Software-Based Image Processing

The remaining image processing steps were implemented using the Matlab programming language. First, each pair of four-plane imageswas re-assembled into a pair of three-plane ones. Spectral sensitivity of the Bayer-patterned CCD varied slightly for the green pixels that were adjacent to either red or blue ones. For the three-plane image, only the red, blue, and red-adjacent green pixels were used.

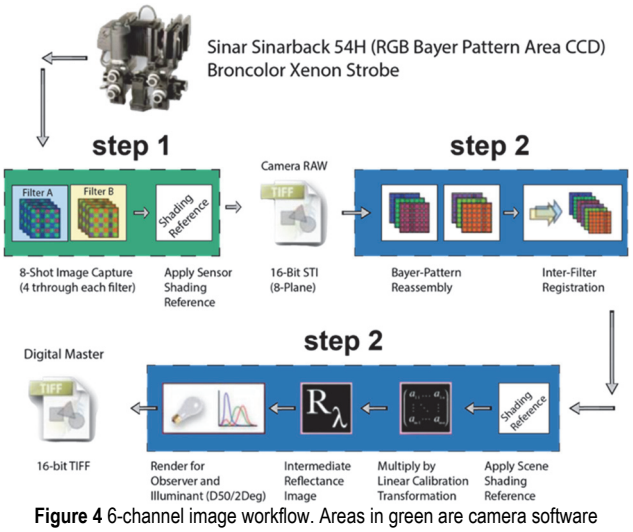

Figure 4 6-channel image workflow. Areas in green are camera software processing, areas in blue are software processing

The physical movement of the two filters resulted in a registration difference between the pair of three-plane images, typically on the order of ten pixels (about 0.25%). Using the public domain software library, ITK [31], and assuming that the images varied only in translation, the images were registered by applying a transformation calculated from a small user-defined region of the image. A multiplicative spatial correction was applied to compensate for spatially non-uniform lighting, commonly used to accentuate surface topography such as impasto. The correction was based on an image of a neutral background, shot under the same conditions as the object. The resulting, final, image was stored in a 16-bit TIFF (CIELAB) image format.

2.4 Wiener Estimation

Wiener estimation is one of the conventional target-based estimation methods. Wiener estimator is optimal in terms of minimizing mean square error when the signal is stationary and the noise is additive. The purpose is to make estimations from a low-dimensional into a high-dimensional data space, in our case forthe 3-channel workflow from three-filter camera responses into reflectance spectra. The approach had to be modified for the implementation on 6-channel images. The goal of this estimation method is to minimize the overall average of the square error between the original and the estimated spectral reflectance. In the study, the Wiener estimation (without considering noise) that provides good accuracy for linear data according to the literature was adopted [32, 34].

The response of a digital camera v_i (x, y) in spatial coordinates (x, y) with i th color filter can be calculated according to Eq. (1),

$$v_i(x,y) = \int u_i(\lambda) S(\lambda) r(x,y;\lambda) d(\lambda) \qquad i = 1, \ldots, m \tag{1}$$

where u_i (λ) is the permeability of the i th filter, E (λ) is the spectrum of the illuminant, S (λ) is the sensitivity of the camera, and r $(x, y; λ)$ is the reflectance spectrum in spatial coordinates (x, y).

In case of images taken by conventional 3-channel RGB camera , m was three, and in case of those captured by modified camera (6 - channel images) m was six.

It is useful to present Eq. (1) in a matrix notation. In this form, the equation is:

$$v = Fr \tag{2}$$

where v is an m-element column vector and r is a k-element column vector which corresponds to the reflectance spectrum of one pixel of an image. In Eq. (2), the r and $v$vectors are related to each other by a linear $(m \times k)$ matrix F. Matrix F is represented by a matrix factorisation as follows:

$$F = UES \tag{3}$$

where,

$$U = \left[u_1, u_2, u_3\right]^T \tag{4}$$

Column vector u_i represents the permetability of the ith filter. In Eq. (3), matrices E (spectrum of the illuminant) and S (sensitivity of the camera) are $(k \times k)$ diagonal matrices.

The solution to Eq. (2) can be found using the linear Wiener estimation method:

$$r_{est} = Gv \tag{5}$$

where v is the RGB response vector and G is the estimation matrix. The purpose of the estimation matrix G is to minimize the minimum square error between original r and estimated r_{est}:

$$e = \left\langle \left| r - r_{est} \right| \right\rangle \rightarrow \min \tag{6}$$

In Eq. (6), signs $\langle\rangle$ mean that the error e is normalized by the amount of used reflectance spectra. Estimation matrix G is explicitly represented as follows:

$$\mathrm{G} = R_{rv} - R_{vv}^{-1} \tag{7}$$

where R_{rv} and R_{vv} are correlation matrices. R_{rv} and R_{vv} are defined as:

$$R_{rv} = \left(rv^t \right), R_{vv} = \left(vv^t \right) \tag{8}$$

In Eq. (8), R_{rv} is the cross-correlation matrix between vectors r and v. Matrix R_{vv} is the autocorrelation matrix of vector v.

The spectral image data $f(x, y, \lambda)$ is calculated from vector v, which is the RGB response, or with vector v including higher order pixel values. In the digital image $f(x, y)$, the matrix G is used as follows:

$$f\left(x, y, \lambda\right) = Gv \tag{9}$$

where G is the estimation matrix. Usage of higher order terms means that instead of using only 3-channel (RGB) and 6-channel values (C_1 to C_6), also second and third-order polynomials were included in the calculations (Tab. 1). For instance, for a 3-channel algorithm with 7 terms, the equation looks as follows: $f(x, y, \lambda) = a_1 \times R + a_2 \times G + a_3 \times B + a_4 \times R^2 + a_5 \times G^2 + a_6 \times B^2 + a_7 \times R \times G \times B$. Here a_1 to a_7 are the corresponding polynomial coefficients, i.e. weights.

Table 1 Number of terms used in the 3-channel (3, 7 or 10) and 6-channel (6, 13 or 69) workflow algorithms

3-channel workflow			6-channel workflow		
3	7	10	6	13	69
R, G, B	R, G, B, R^2, G^2, B^2, $R \times G \times B$	R, G, B, R^2, G^2, B^2, $R \times G$, $G \times B$, $R \times B$, $R \times G \times B$	c_1, c_2, c_3, c_4, c_5, c_6	c_1, c_2, c_3, c_4, c_5, c_6, c_1^2, c_2^2, c_3^2, c_4^2, c_5^2, c_6^2 $c_1 \times c_2 \times c_3 \times c_4 \times c_5 \times c_6$	c_1, c_2, c_3, c_4, c_5, c_6, $c_1 \times c_2$, …, $c_5 \times c_6$, $c_1 \times c_2 \times c_3$, …, $c_4 \times c_5 \times c_6$, $c_1 \times c_2 \times c_3 \times c_4$, …, $c_3 \times c_4 \times c_5 \times c_6$, $c_1 \times c_2 \times c_3 \times c_4 \times c_5$, …, $c_2 \times c_3 \times c_4 \times c_5 \times c_6$, $c_1 \times c_2 \times c_3 \times c_4 \times c_5 \times c_6$

2.5 Workflow

2.5.1 Three and Six Channel Procedure

In the 3-channel workflow conventional SinarBack 54 FO Digital RGB camera was used for capturing Color Chart DC patches illuminated under 45° by Broncolor Pulso G Flashlights. In case of the 6-channel workflow the modified Sinar Back 54 FO Digital camera was implemented and the Color Chart DC was illuminated under 45° by Broncolor HMI F1200 lights.

With both workflows, all 240 patches were first measured with i1Pro spectrophotometer to get spectral reflectance data and then randomly split into 160 training and 80 testing samples. Following the machine learning approach, the training sets were used for creating reflectance reconstruction models while the models' performance was assessed using the testing sets by means of three quality metrics as described below.

2.6 Quality Metrics

In our research three metrics for assessing the quality of spectral reflectance reconstruction were implemented: root-mean-square-error (*RMSE*), peak-signal-to-noise-ratio (*PSNR*) and colorimetric color difference (CIE *DE*2000).

2.6.1 *RMSE* and *PSNR*

RMSE and *PSNR* are two related measures of the differences (= errors) between the observed, i.e. measured, and the predicted, i.e. reconstructed, image. (Eq. (10) and Eq. (11)). The lower the *RMSE* (and the higher the *PSNR*), the better the image is reconstructed to match the original one and the better the corresponding algorithm. The main limitation of both metrics is that they rely strictly on numeric comparison and do not take into account any level of biological factors of the human vision system or human opinion. While these metrics can provide a quantitative measure of image quality, they may not always correspond to the perceptual quality of an image as perceived by a human observer.

$$RMSE = \sqrt{\sum_{i=1}^{n} \frac{\left(y_i - \hat{y}_i \right)^2}{n}} \tag{10}$$

$$PSNR = 20\log_{10}\left(\frac{\mathrm{MAX}}{RMSE} \right) \tag{11}$$

2.6.2 CIE *DE*2000

With CIE *DE*2000 we can present the color difference between the measured and the reconstructed values of color patches (Eq. (12)). First *XYZ* values were computed from the measured and the recontructed spectra of patches followed by the calculation of LAB values using the defined whitepoint *D*50, i.e. daylight (5000 K).

Compared with the CIE Lab formula, the CIE *DE*2000 formula is more advanced and more accurate. It redefines the calculation of color difference so that the results are closer to the evaluation of human eyes. CIE *DE*2000 introduces three new terms S_L, S_C, and S_H representing the

degree of differences in the direction of lightness (ΔL^*), chroma (ΔC^*) and hue (ΔH^*). It also includes three constant coefficients, namely k_L, k_C and k_H. In general, when comparing two colors using the CIE *DE*2000 formula, a lower ΔE value indicates a smaller color difference and a higher level of color similarity between the two colors [35].

$$\Delta E_{00}^{*}=\sqrt{\left(\frac{\Delta \mathrm{L}}{k_L S_L}\right)^2+\left(\frac{\Delta \mathrm{C}}{k_C S_C}\right)^2+\left(\frac{\Delta \mathrm{H}}{k_H S_H}\right)^2+R_T \frac{\Delta \mathrm{C}}{k_C S_C} \frac{\mathrm{a} \Delta \mathrm{H}}{k_H S_H}} \quad (12)$$

3 RESULTS AND DISCUSSION

A number of mathematical models were built in order to address the research questions given in the Introduction. Tab. 2 shows average values of *RMSE*, *PSNR* and *DE*2000 of 80 test sample patches for 3 and 6-channel workflows and different numbers of terms. In general, we can say that when reconstructing images with a larger number of channels (6 compared to 3), better results as assessed by *RMSE*, *PSNR* and *DE*2000 are obtained. The same applies to the number of terms in the reconstruction algorithm as the number of terms increases, the results generally improve. When the number of terms in the 6 - channel algorithm increased from 13 to 69, however, the results became significantly worse. This decrease in performance when using a larger number of terms may be due to overfitting, which occurs when a model is too complex and begins to fit the noise in the data rather than the underlying patterns.This well known machine learning phenomenon takes place when the model gives accurate predictions for training data but not for new, i.e. test, data.

Table 2 Mean values of 80 test sample patches for 3 and 6-channel workflows and different terms

	No. of terms					
	3-channel workflow			6-channel workflow		
quality metrics	3	7	10	6	13	69
RMSE	0.079	0.045	0.032	0.031	0.027	0.026
PSNR	71.286	76.509	79.371	79.674	81.368	82.044
*DE*2000	7.13	3.937	3.364	1.97	1.779	3.359

To determine whether there is a statistically significant difference between the means within the 3-channel as well as within the 6-channel algorithms for each of the three quality metrics, *t*-test for independent samples was performed (Tab. 3). Alternatively, where the variables were not normally distributed, its non-parametric equivalent Mann-Whitney U test was used; normality was checked using the Lilliefors test. The significant level (alpha) was 0.05.

The table shows that for the 3-channel algorithm there is a statistically significant difference (p-val < 0.05) between the 7 and 10-term models (yellow) for *RMSE* and *PSNR*. Although this is not the case for the CIEDE2000 metrics, we decided to keep the 10-term model, since it is charaterized by the lowest *RMSE* and CIE *DE*2000 and the highest *PSNR* values. When considering the 6-channel algorithm, no significant difference between the 6 and 13-terms models (orange) was detected with any of the three quality metrics. Nevertheless, as with the 3-channel algorithm, we used in our further calculations the more complex model with 13 terms due to its lower *RMSE* and CIE *DE*2000 and higher *PSNR* values.

Table 3 Statistical assessment of differences between the means of individual 3 and 6-channel models for each of the three metrics

Var1	Var2	Var1 mean	Var2 mean	test	p-val
c3_t3_*RMSE*	c3_t7_*RMSE*	0.079	0.045	M-W U	< 0.01
c3_t3_*RMSE*	c3_t10_*RMSE*	0.079	0.032	M-W U	< 0.01
c3_t7_*RMSE*	c3_t10_*RMSE*	0.045	0.032	M-W U	0.013
c6_t6_*RMSE*	c6_t13_*RMSE*	0.031	0.027	M-W U	0.273
c6_t6_*RMSE*	c6_t69_*RMSE*	0.031	0.026	M-W U	0.192
c6_t13_*RMSE*	c6_t69_*RMSE*	0.027	0.026	M-W U	0.799
c3_t3_*PSNR*	c3_t7_*PSNR*	71.286	76.509	M-W U	< 0.01
c3_t3_*PSNR*	c3_t10_*PSNR*	71.286	79.371	*t*-test	< 0.01
c3_t7_*PSNR*	c3_t10_*PSNR*	76.509	79.371	M-W U	0.013
c6_t6_*PSNR*	c6_t13_*PSNR*	79.674	81.368	*t*-test	0.187
c6_t6_*PSNR*	c6_t69_*PSNR*	79.674	82.044	*t*-test	0.087
c6_t13_*PSNR*	c6_t69_*PSNR*	81.368	82.044	*t*-test	0.652
c3_t3_*dE*2000	c3_t7_*dE*2000	7.13	3.937	M-W U	< 0.01
c3_t3_*dE*2000	c3_t10_*dE*2000	7.13	3.364	M-W U	< 0.01
c3_t7_*dE*2000	c3_t10_*dE*2000	3.937	3.364	M-W U	0.516
c6_t6_*dE*2000	c6_t13_*dE*2000	1.97	1.779	M-W U	0.458
c6_t6_*dE*2000	c6_t69_*dE*2000	1.97	3.359	M-W U	0.571
c6_t13_*dE*2000	c6_t69_*dE*2000	1.779	3.359	M-W U	0.189

Next, we wanted to get more insight into the models' performance for various types of color patches, specifically skin, neutral and saturated tones, to see how successful is the algorithm when encountering extreme differences in color characteristics, such as hue or saturation. Fig. 5 to Fig. 7 show results of quality metrics (*RMSE*, *PSNR* and *DE*2000) calculated for the 3-channel-10-terms model and the 6-channel-13-terms model, for the saturated, neutral, and skin tones, respectively. For individual patch codes, see Fig. 3.

Fig. 5 shows that in general *RMSE* is the lowest corresponding to the best model performance for the neutral tones, followed by the skin tones and the saturated patches, for both 3 and 6-channel workflows. As can be expected, the highest *PSNR* values (Fig. 6) were also found with neutral and the lowest with the saturated color samples. When examining *DE*2000 results (Fig. 7), however, the lowest color difference was found with the skin patches, followed by the neutral and the saturated ones.

When studying Fig. 7, it can be observed that the patches *L*8, *K*8, and *J*8 have very high values of *DE*2000 for the 3-channel workflow. These patches are the darkest within the selection of neutrals, so it is possible to predict that the brightness (L^*) negatively correlates with the color difference *DE*2000 in the case of neutral tones.

These results can be better understood by examining the shape of the measured and reconstructed spectra, which are presented in Fig. 8 to Fig. 10. We can see that the saturated patches have highly diverse spectra, with numerous peaks and local maxima, in contrast to the neutral patches that have smoother curves. These variations in the shape of the saturated patches' spectra could make it more challenging for the algorithm to adapt, especially compared to the neutral spectra that exhibit more uniformity with less fluctuations.

When examining the saturated patches (Fig. 8 to Fig. 10), the poorest result in terms of *DE*2000 for both 3 and 6- channel images was obtained for patch S4 (11.7 and 13.1, respectively). On the other hand, the best

performances within 3 and 6-channel images were observed for S8 (2.2) and S9 (2.6), respectively.

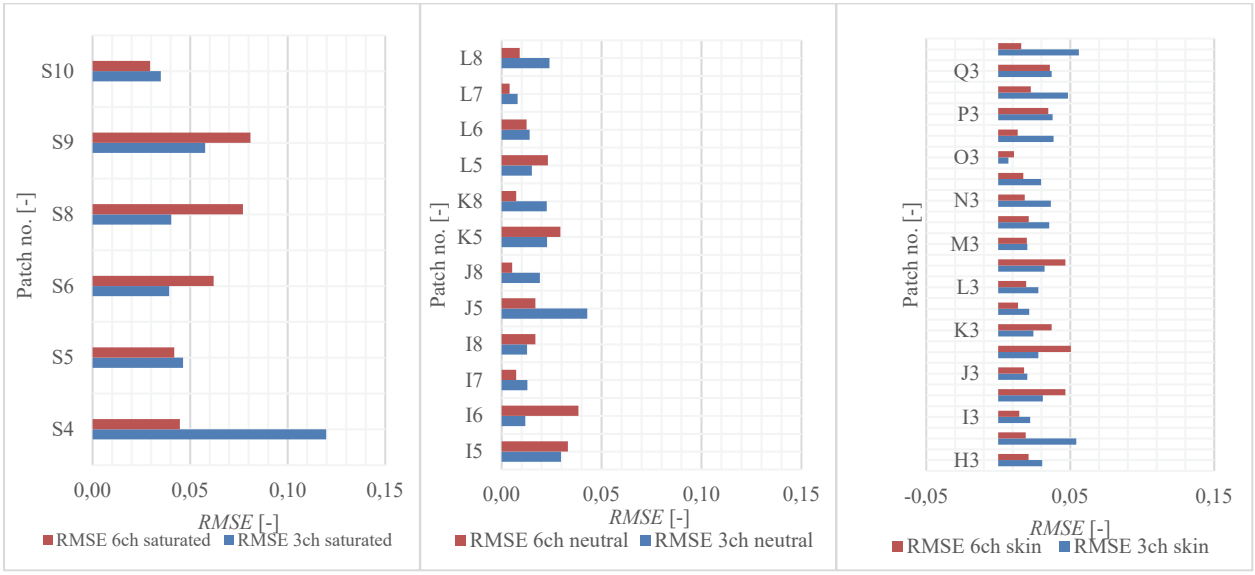

Figure 5 *RMSE* for 3 and 6-channel algorithm for saturated, neutral and skin patches of color chart Color Checker DC

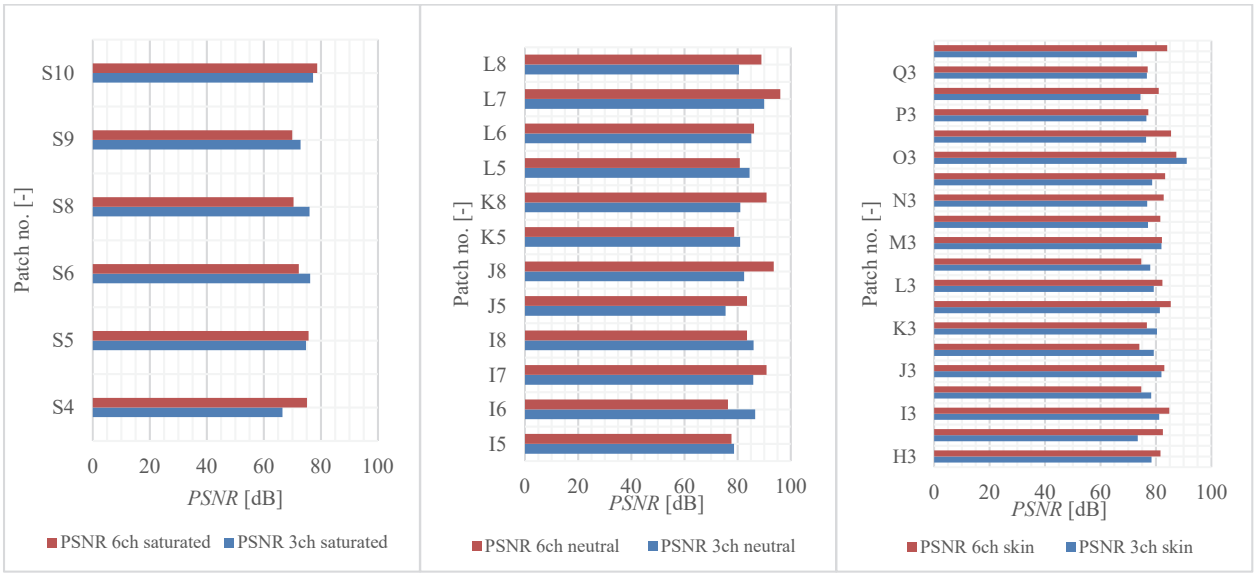

Figure 6 *PSNR* for 3 and 6-channel algorithm for saturated, neutral and skin patches of color chart Color Checker DC

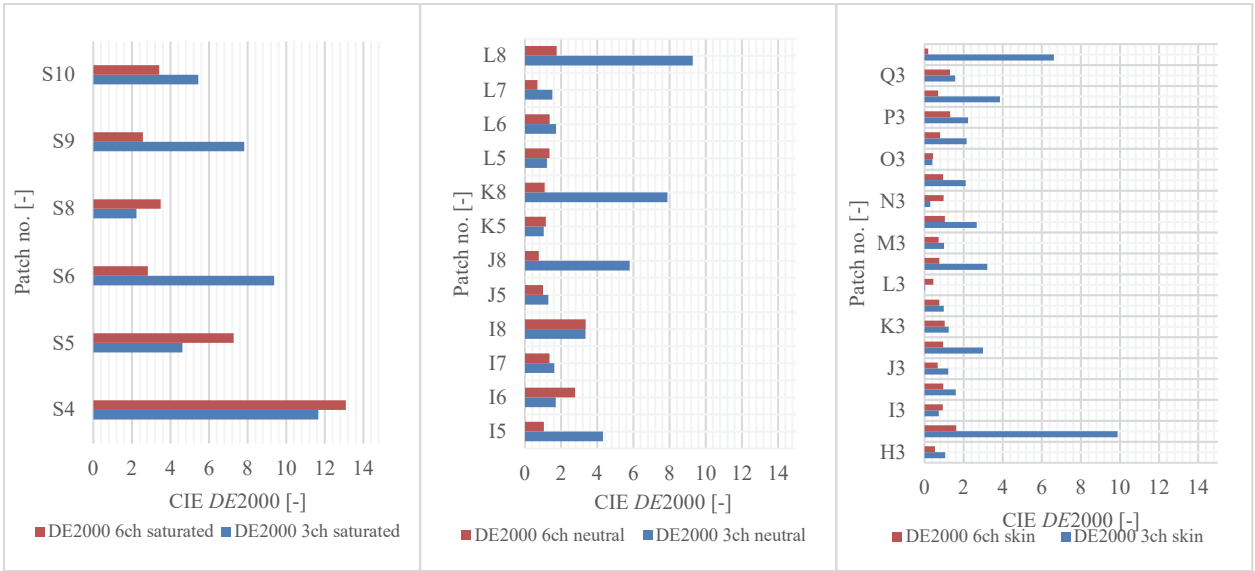

Figure 7 *DE*2000 for 3 and 6-channel algorithm for saturated, neutral and skin patches of color chart Color Checker DC

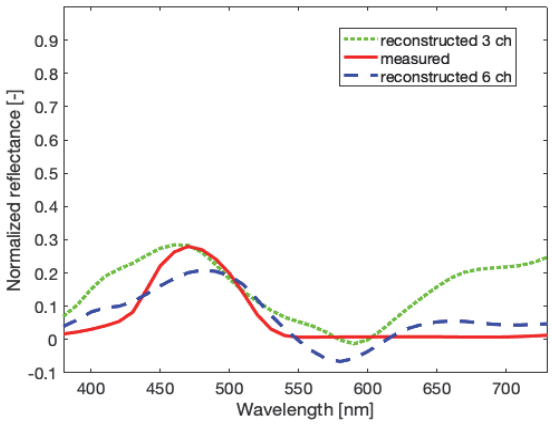

Figure 8 Comparison of reconstructed and measured spectra for the saturated patch S4

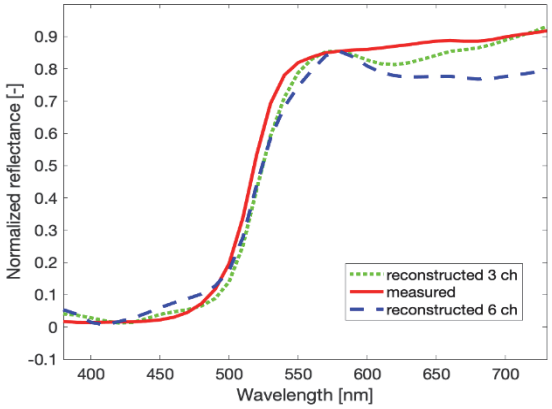

Figure 9 Comparison of reconstructed and measured spectra for the saturated patch S8

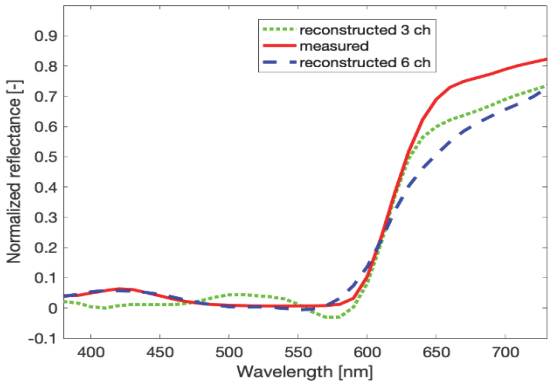

Figure 10 Comparison of reconstructed and measured spectra for the saturated patch S9

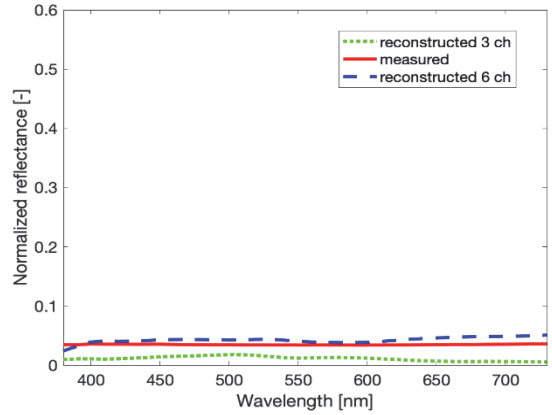

Figure 11 Comparison of reconstructed and measured spectra for the neutral patch L8

Regarding the neutral patches (Fig.11 to Fig. 14), the poorest result in terms of *DE*2000 for 3-channel images was obtained for patch L8 (9.3), and for 6-channel images for patch I8 (3.4). The best performances for 3 and 6-channel images were found for patches K5 (1.0) and L7 (0.7), respectively.

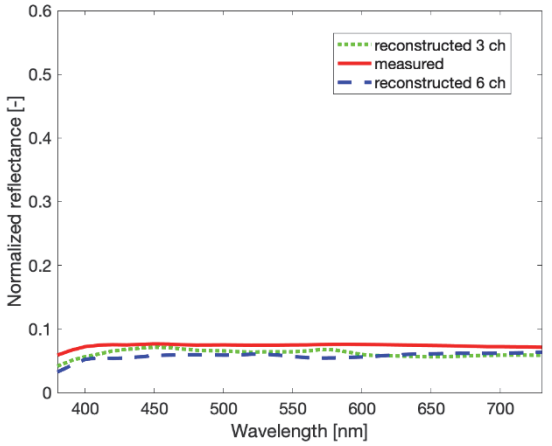

Figure 12 Comparison of reconstructed and measured spectra for the neutral patch I8

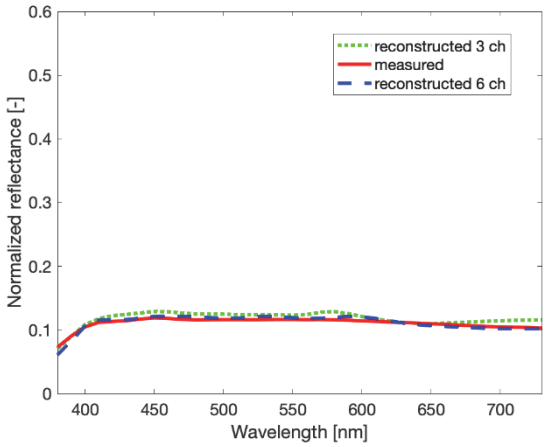

Figure 13 Comparison of reconstructed and measured spectra for the neutral patch L7

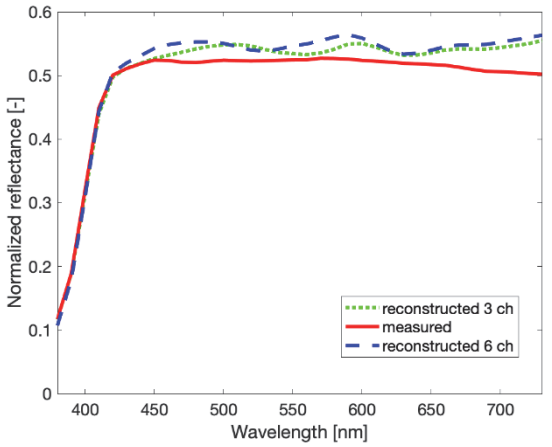

Figure 14 Comparison of reconstructed and measured spectra for the neutral patch K5

When focusing on the skin patches (Fig. 15 to Fig. 17), the poorest result in terms of *DE*2000 for both 3 and 6-channel images was obtained for patch H4 (9.9 and 1.6, respectively). The best performance within 3-channel

images was found for patch L3 (0.04) and for 6-channel image for patch Q4 (0.19).

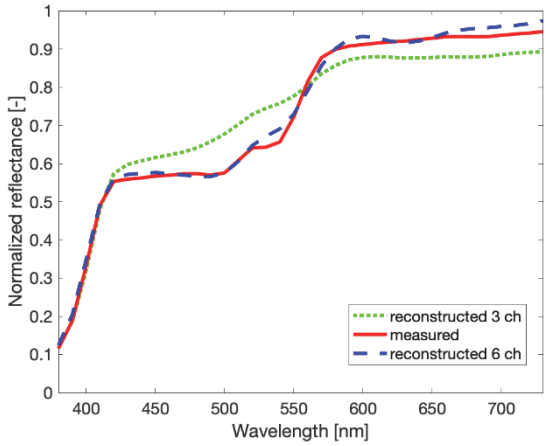

Figure 15 Comparison of reconstructed and measured spectra for the skin tone patch Q4

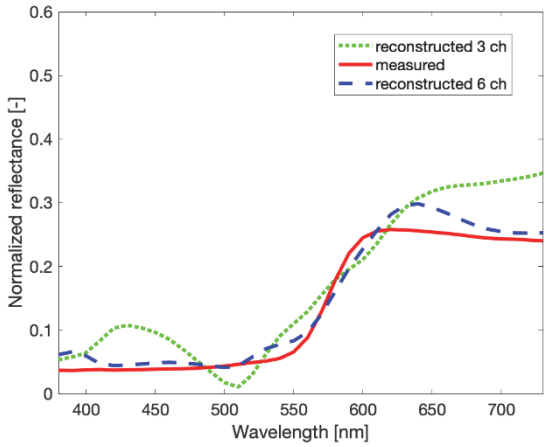

Figure 16 Comparison of reconstructed and measured spectra for the skin tone patch H4

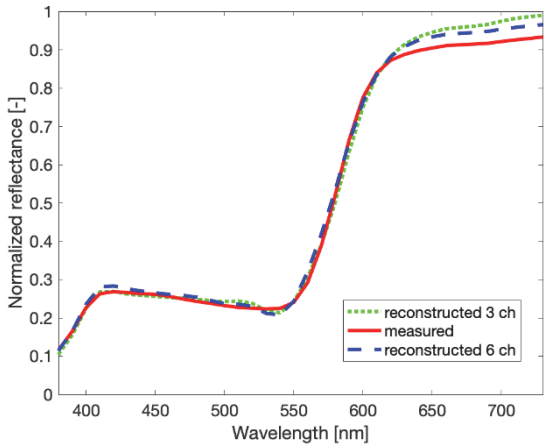

Figure 17 Comparison of reconstructed and measured spectra for the skin tone patch L4

4 CONCLUSION

In the study we estimated an optimal number of terms in the computational algorithm that led to the best results in terms of image reconstruction quality. When using 10 terms the best results were obtained for the 3-channel images, while using 13 terms led to the best performance for the 6-channel images. It was also found that increasing the number of terms beyond 13 for 6-channel images led to a drastic decrease in model performance, probably due to overfitting.

We found out in the research that the best results in terms of color difference (*DE*2000) were calculated for the skin tones, followed by the neutral and saturated patches for both 3 and 6-channel algorithms. Similar results were found in the previous studies [33]. This may be related to the shape of the spectr saturated patches have very varied spectra, with peaks and local maxima, which can be considered to make the algorithm more difficult to adapt, then for example in the case of neutral spectra, where the curves are very smooth, without stronger variations in the shape of the spectrum.

Results of the study are applicable to various graphics-oriented applications, for instance they can be used in a printing workflow where a high precision color rendering is required or for accurate digitization of paintings and other works of art.

For a better understanding, we suggest further research, that can enhance our understanding of the mentioned issues, e.g. by improving noise modelling. By exploring different methods for estimating spectra, we can gain new insights and potentially improve the accuracy and reliability of our results. Increasing the number of dataset samples could also contribute to a more comprehensive and robust analysis.

5 REFERENCES

[1] Rosen, M. R. (2023) Spectral Imaging. *Free Encyclopedia, Net Industries and its Licensors.*

[2] Hardeberg, J. Y. (1999). *Acquisition and reproduction of color images: colorimetric and multispectral approaches:* Ph.D. dissertation. Ecole Nationale Superieure des Telecommunications, 1-302.

[3] Cheung, V., Westland, S., Li, C., Hardeberg, J., & Connah, D. (2005). Characterization of trichromatic color cameras by using a new multispectral imaging technique. *Journal of the Optical Society of America A*, *22*(7), 1231-1240. https://doi.org/10.1364/JOSAA.22.001231

[4] Fairchild, M., Rosen, M., & Johnson, G. M. (2001). Spectral and Metameric Color Imaging. *Physics*, 1-8.

[5] Maitre, H., Schmitt, F., Crettez, J. P, Wu, Y., & Hardeberg, J. Y. (1996). Spectrophotometric Image Analysis of Fine Art Paintings. *IS&T/SID 4th Color Imaging Conference*, 50-53.

[6] Berns, R. S. (2005). *Scientific examination of art: Modern techniques in conservation and analysis: Color-Accurate Image Archives Using Spectral Imaging.* National Academies Press.

[7] Berns, R. S., Zhao, Y., Taplin, L. A., Coddington, J., McGlinchey, C., & Martins, A. (2009). The Use of Spectral Imaging as an Analytical Tool for Art Conservation. *American Institute of Conservation, Annual Meeting, Los Angeles, California, United States*, 1-50.

[8] Berns, R. S., Taplin, L .A., Nezamabadi, M., Zhao, Y., & Okumura, Y. (2005). High-Accuracy Digital Imaging of Cultural Heritage without Visual Editing. *IS&T's 2005 Archiving Conference, Washington*, DC, 91-95.

[9] Taplin, L. A. & Berns, R. S. (2005). Practical spectral capture systems for museum imaging. *Proc. of the 10th Congress of the International Colour Association, Granada, Spain,* 1287-1290.

[10] Swain, P. H. & Davis, S. M. (1978). *Remote sensing: The quantitative approach.* McGraw-Hill International Book.

[11] Lillesand, T. & Kiefer, R. W. (1995). Remote Sensing and Image Interpretation. *Geological Magazine*, *132*(2) 248-

249.
[12] Tsumura, N., Kawabuchi, M., Haneshi, H., & Miyake, Y. (2000). Mapping Pigmentation in Human Skin by Multi-Visible- Spectral Imaging by Inverse Optical Scattering Technique. *IS&T/SID 8th Color Imaging Conference,* 81-84.
[13] Hege, E. K., O'Connell, D., Johnson, W., Basty, S., & Dereniak, E. L. (2004). Hyperspectral imaging for astronomy and space surveillance. *Proceedings of SPIE - The International Society for Optical Engineering*, *5159*, 1-12. https://doi.org/10.1117/12.506426
[14] Haneishi, H., Hasegawa, T., Hosoi, A., Yokoyama, T., Tsumura, N., & Yoichi, M. Y. (2000). System Design for Accurately Estimating the Spectral Reflectance of Art Paintings. *Applied Optics*, *39* (35), 6621-6632.
[15] Seymour, J. (2009). Color measurement with an RGB camera*. Physics,* 1-28.
[16] Hong, G., Luo, M. R., & Rhodes, P. A. (2001). A study of digital camera colorimetric characterization based on polynomial modeling. *Color Research and Application*, *26*(1), 76-84. https://doi.org/10.1002/15206378(200102)26:1<76::AIDCOL8>3.0.CO;2-3
[17] Barnard, K. & Funt, B. (2002). Camera characterization for color research. *Color Research and Application*, *27*(3), 153-164.
[18] Lazar, M. & Hladnik, A. (2022). Exploiting nonlinearity between parallel channels of multiple cameras for accurate ANN reconstruction of reflectance spectra. *Tehnički vjesnik, 29* (3), 765-774. https://doi.org/10.17559/TV-20210405174515
[19] Lazar, M., Javoršek, D., Hladnik, A. (2020). Study of camera spectral reflectance reconstruction performance using CPU and GPU artificial neural network modelling. *Tehnički vjesnik*, *27* (4), 1204-1212. https://doi.org/10.17559/TV-20190526202030
[20] Liu, Y., Yu, H. & Shi, J. (2008). Camera characterization using back-propagation artificial neutral network based on Munsell system. *International Symposium on Photoelectronic Detection and Imaging: Photoelectronic Imaging and Detection*, *6621*, 1-12. https://doi.org/10.1117/12.790592
[21] Cheung, V. & Westland, S. (2003). An Evaluation of Multispectral Imaging Techniques for Camera Characterization*. The Eleventh Color Imaging Conference: Color Science and Engineering Systems, Technologies, Applications, Scottsdale, Arizona, USA,* 193-198.
[22] Maloney, L. T. (1986). Evaluation of linear models of surface spectral reflectance with small numbers of parameters. *Journal of the Optical Society of America A,* 3 (10), 1673-1683. https://doi.org/10.1364/JOSAA.3.001673
[23] Morovic, P. & Finlayson, G. D. (2006). Metamer-set-based approach to estimating surface reflectance from camera RGB. *Journal of the Optical Society of America A, 23*(8), 1814-1822. https://doi.org/10.1364/JOSAA.23.001814
[24] Nieves, J. L., Valero, E. M, Nascimento, S., Hernández-Andrés, J., & Romero, J. (2005). Multispectral synthesis of daylight using a commercial digital CCD camera*. Applied Optics, 44*(27), 5696-5703. https://doi.org/10.1364/AO.44.005696
[25] Imai, F. H. & Berns, R. S. (1999). Spectral estimation using trichromatic digital cameras. *Proceedings of the International Symposium on Multispectral Imaging and Color Reproduction for Digital Archives*, 42-49.
[26] Hu, Y., Hernández-Andrés, J., Nieves, J. L., Valero, E. M., Romero, J., Schnitzlein, M., & Nowack, D. (2011). Evaluation and optimization of spectral estimation algorithms for printer inks. *Proceedings of the International Color Assocciation*, 422-427.
[27] Heikkinen, V., Lenz, R., Jetsu, T., Parkkinen, J., Hauta-Kasari, M., & Jääskeläinen, T. (2008). Evaluation and unification of some methods for estimating reflectance spectra from rgb images. *JOSAA, 25*(10), 2444-2458. https://doi.org/10.1364/JOSAA.25.002444
[28] Shimano, N., Terai, K., & Hironaga, M. (2007). Recovery of spectral reflectances of objects being imaged by multispectral cameras. *Journal of the Optical Society of America A, 24*(10), 3211-3219. https://doi.org/10.1364/JOSAA.24.003211
[29] Berns, R. S., Taplin, L. A., & Nezamabadi, M. (2004). Modifications of a sinarback 54 digital camera for spectral and high-accuracy colorimetric imaging: simulations and experiments. *Physics.* 1-24.
[30] Berns, R. S., Urban, P., & Rosen, M. R. (2008). A Spatially Adaptive Wiener Filter for Reflectance Estimation. *IS&T/SID, 16th Color Imaging Conference, Portland, Oregon.*, 1-7. https://doi.org/10.2352/CIC.2008.16.1.art00053
[31] Ibáñez, L., Schroeder, W., Ng, L., & Cates, J. (2003). *TheITK Software Guide. 2nd ed.* Kitware.
[32] Tominaga, S. & Sakai, H. (2023). Spectral Reflectance Estimation from Camera Responses Using Local Optimal Dataset. *J. Imaging*, *9*(2), 47. https://doi.org/10.3390/ jimaging9020047
[33] Stigell, P., Miyata, K., & Hauta-Kasari, M. (2007). Wiener estimation method in estimating of spectral reflectance from RGB images. *Pattern Recognition and Image Analysis*, *17*(2), 233-242.
[34] Shen, H. L., Cai, P. Q., Shao, S. J., & John, H. X. (2007). Reflectance reconstruction for multispectral imaging by adaptive Wiener estimation. *Optics Express*, *15*(23), 15545-54.
[35] Sharma, G., Wu, W., & Dalal, E. N. (2005). The CIEDE2000 Color-Difference Formula: Implementation Notes, Supplementary Test Data, and Mathematical Observations. *Color Research & Application*, *30*(1), 21-30.

Contat information:

Andrej UČAKAR, B.Sc. Graf. technol.
(Corresponding author)
University of Ljubljana,
Faculty of Natural Sciences and Engineering,
Department of Textiles, Graphic Arts and Design,
Snežnka ulica 5, SI-1000 Ljubljana, Slovenia
E-mail: andrej.ucakar@ntf.uni-lj.si

Primož WEINGERL, Assistant, PhD
University of Ljubljana,
Faculty of Natural Sciences and Engineering,
Department of Textiles, Graphic Arts and Design,
Snežniška ulica 5, SI-1000 Ljubljana, Slovenia
E-mail: primoz.weingerl@ntf.uni-lj.si

Andrej KOŠIR, Professor, PhD
University of Ljubljana,
Faculty of Electrical Engineering,
VIII. ICT Department,
Tržaška cesta 25, SI-1000 Ljubljana, Slovenia
E-mail: andrej.kosir@fe.uni-lj.si

Aleš HLADNIK, Associate Professor, PhD
University of Ljubljana,
Faculty of Natural Sciences and Engineering
Department of Textiles, Graphic Arts and Design,
Snežniška ulica 5, SI-1000 Ljubljana, Slovenia
E-mail: ales.hladnik@ntf.uni-lj.si